Published in final edited form as:
Eur J Neurosci. 2005 May ; 21(10): 2660–2670. doi:10.1111/j.1460-9568.2005.04086.x.

Temporal pattern of plasma membrane calcium ATPase 2 expression in the spinal cord correlates with the course of clinical symptoms in two rodent models of autoimmune encephalomyelitis

Arnaud Nicot[1,2,3], **Michael Kurnellas**[1,2], and **Stella Elkabes**[1,2]

[1]University of Medicine and Dentistry of New Jersey, New Jersey Medical School, Department of Neurology and Neuroscience, Newark, NJ, United States

[2]Veterans Affairs, Neurology Service, East Orange, NJ, United States

[3]Inserm U732, Hôpital Saint-Antoine, 75012 Paris, France

Abstract

Axonal/neuronal pathology is an important and early feature of multiple sclerosis and its animal model, experimental autoimmune encephalomyelitis (EAE). However, the underlying molecular mechanisms remain elusive. We have previously reported that the levels of an important neuronal calcium pump, plasma membrane calcium ATPase 2 and synaptic proteins, synapsin IIa and syntaxin 1B are decreased in the rat spinal cord at onset of acute EAE. Whether the expression of these genes is restored during neurological recovery and affected in other EAE models is currently unknown. The present study was undertaken to address these issues by use of validated multiplex quantitative real-time RT-PCR with fluoro-primers, western blot and immunocytochemistry. We report that plasma membrane calcium ATPase 2 (PMCA2) transcript and protein levels return to control values during recovery from acute disease in the Lewis rat, whereas they are reduced throughout the course of chronic, non-remitting EAE in the C57Bl/6 mouse. These results indicate a close correlation between PMCA2 levels and disease course as defined by clinical scores reflecting motor deficits. Decrease in synapsin IIa expression also correlated with the onset and progression of neurological symptoms, whereas the pattern of syntaxin 1B mRNA and protein expression suggested post-transcriptional regulation. The decrease in PMCA2 transcript and protein levels and the correlation between expression and disease course in two different EAE models further highlight the importance of this calcium pump in neuronal dysfunction during inflammation.

Keywords

Atp2b2; neuroinflammation; neuronal transcripts; Syn2; Stx1

Introduction

Experimental autoimmune encephalomyelitis (EAE) is one of the best-characterized animal models of multiple sclerosis (MS). It is induced in rodents by immunization with myelin-derived peptides and spinal cord homogenates or by adoptive transfer of encephalogenic T-

Correspondence: Dr Arnaud Nicot, Inserm U732, Hôpital Saint-Antoine, 75012 Paris, France nicot@st-antoine.inserm.fr.

cells. The use of different animal species or strains and immunization protocols results in distinct disease course and diverse pathological features that mimic various aspects of MS (Wekerle *et al.*, 1994; Weissert *et al.*, 1998; van der Goes & Dijkstra, 2001; Storch *et al.*, 2002). Lewis rats inoculated with myelin basic protein (MBP) develop either a mild disease followed by recovery of function or severe symptoms, depending on the immunization protocol used (Imrich & Harzer, 2001). In this model, demyelination is little or absent. The C57Bl/6 mice develop chronic EAE with symptoms lasting for several weeks when immunized with myelin oligodendrocyte glyco-protein $(MOG)_{35–55}$. Demyelination is one of the hallmarks of this model.

Despite the diversity in disease course and variability in demyelination, a feature common to all models of EAE is the presence of axonal pathology (White & Bowker, 1988; Pitt *et al.*, 2000; Smith *et al.*, 2000; Ahmed *et al.*, 2001; Zhu *et al.*, 2003). Initially, axonal damage was thought to occur at later stages of EAE or MS as a consequence of demyelination. Recent studies challenge this concept, as magnetization transfer ratio, an index of demyelination, does not correlate with the loss of *N*-acetyl aspartate, an index of axonal injury (Pendlebury *et al.*, 2000). Moreover, axonal damage is detectable at the earliest clinical stage and is best correlated with inflammation (Kuhlmann *et al.*, 2002; Filippi *et al.*, 2003). The studies on MBP-induced acute EAE in the Lewis rat are in agreement with these latter findings as axonal pathology is observed in the absence of demyelination (Smith *et al.*, 2000).

Several issues relating to neuronal/axonal damage remain poorly understood. Are mechanisms of axonal pathology reversible? Do permanent molecular changes occur despite recovery of function? Are the molecular changes underlying neuronal/axonal pathology similar in different EAE models? The present studies were undertaken in order to provide insights into some of these questions. We had previously shown that the expression of several genes and especially PMCA2, synapsin IIa and syntaxin 1B were decreased at onset of acute EAE in the Lewis rat (Nicot *et al.*, 2003). As PMCAs are major pumps that extrude calcium from cells whereas synapsin IIa and syntaxin 1B mediate vesicular trafficking and exocytosis, respectively (Rosahl *et al.*, 1995; Garcia & Strehler, 1999; Hilfiker *et al.*, 1999; Lin & Scheller, 2000), alterations in the expression of these genes may underlie neuronal pathology. The current investigations assessed how the expression of the aforementioned neuronal genes is modulated during the entire clinical course of the disease in the Lewis rat, including the recovery period. We also determined whether the expression of these genes is affected in the $MOG_{35–55}$-induced EAE in C57Bl/6 mice, a disease characterized by demyelination, axonal damage and irreversible symptoms. The present findings indicate that changes in PMCA2 mRNA and protein levels correlate with the course of clinical symptoms in two models of EAE. These results further support a role for aberrant calcium extrusion in neuronal pathology during spinal cord inflammation.

Materials and methods

Induction of EAE in the Lewis rat and C57Bl/6 mouse

Female adult Lewis rats (8–10 weeks old, Charles River, Wilmington, MA) were anaesthetized with isoflurane and the hindlimb footpad was inoculated with 100 μL of an emulsion containing 100 μg guinea pig myelin basic protein (Sigma, St Louis, MO, USA) in saline and an equal volume of complete Freund's adjuvant (CFA) supplemented with 200 μg mycobacterium tuberculosis H37RA (Difco, Detroit, MI, USA). Control rats received only saline/adjuvant. C57BL/6J mice (8 weeks old, Charles River, MA, USA) were immunized subcutaneously in two sites (flank and footpad) with 50 μL of an emulsion containing 200 μg $MOG_{35–55}$ in saline and an equal volume of complete Freund's adjuvant containing 175 μg mycobacterium tuberculosis H37RA (Difco Laboratories, Detroit, MI, USA) under isoflurane anaesthesia. Control mice received saline/adjuvant. Three hundred nanograms of pertussis toxin (List

Biologicals, Campbell, CA, USA) was administrated i.p. at 0 and 48 h after immunization. Animals were given food and water *ad libitum* and were monitored daily for clinical symptoms. EAE was characterized by ascending paralysis beginning with tail flaccidity. Neurological impairment was scored as: 0, no neurological symptoms (E0); 0.5, tail flabbiness; 1, tail paralysis (E1); 1.5, weakness in one hindlimb; 2, weakness in both hindlimbs or one hindlimb paralysis (E2); 2.5, one hindlimb paralysis and weakness in other hindlimb; 3, paralysis of both hindlimbs (E3). Some animals were killed by exposure to CO_2/O_2, the lumbar spinal cords were dissected out and frozen on dry ice. Others were perfused as described below. The tissue was kept at) −80 °C until further use. All animal procedures were performed according to IACUC and institutional guidelines. Mice or rats (< 10%) that did not develop EAE on the expected days were excluded from the study. Animals were given easy access to food and water during experiments. To follow institutional guidelines, animals that reached a clinical score higher than 3 and developed quadriplegia for more than one day, were killed by exposure to CO_2/O_2.

Tissue collection

The lumbar spinal cord of rats was divided into two segments. One of the fragments was used for RNA extraction and the other for crude membrane preparation. A total of nine to ten controls and 17 EAE rats at different disease stages (n = 3–5 per group) were used for real-time PCR and western blot analysis. A total of eight controls and 25 EAE mice at different disease stages (n = 5–8 per group) were used for real-time PCR. Four controls and four EAE mice on day 24 post-immunization (PI; clinical score 2.5–3) were used for western blot analysis.

cDNA preparation

Total RNA was extracted from each lumbar spinal cord (10–15 mg) using the RNAqueous isolation kit (Ambion, Austin, TX, USA). Residual genomic DNA was removed by incubating the RNA sample with RNase-free DNase I (Ambion). DNase-treated total RNA (0.5–1 μg) was reverse-transcribed by MMV-RT along with random primers and 40 U RNAse inhibitor (Ambion), in a total reaction volume of 20 μL according to the manufacturer's instruction.

Semi-quantitative RT-PCR for the evaluation of PMCA1, 3 and 4 expression

Five microlitres of the reverse transcription product was amplified in a total volume of 50 μL using SuperTaq™ Polymerase (Ambion) according to the manufacturer's instructions. Primers specific for PMCA1, 3 or 4 (Fresu *et al.*, 1999) were used. Alpha-tubulin, a housekeeping gene not modulated during acute EAE (Nicot *et al.*, 2003) was used as the internal control to normalize for variations in experimental differences. PCR was performed for 30 cycles within the linear range (denaturation, 1 min at 94 °C, annealing, 1 min at 58 °C and extension 1 min at 72 °C). Products were separated on a 1.3% agarose gel in Tris-acetate-EDTA Buffer containing ethidium bromide (0.5 μg/mL). A 15 μL aliquot of the PCR products was loaded on the gel. Images were captured using ChemiImager digital imaging system (Alpha Innotech, San Leandro, CA, USA). The optical density in each band was quantified using the Un-Scan-It software (Silk Scientific, Orem, UT, USA).

Real-time PCR using fluorogenic LUX primers

The primers for quantitative real-time PCR were designed using Lux Primer software (Invitrogen, San Diego, CA, USA), based on the published rat and mouse mRNA and genomic DNA sequences in GenBank. Primers used in the present study are rat and mouse gene-specific as confirmed by the BLAST search. Amplified fragments are sequence 983–1062 of PMCA2 cDNA (GenBank access number J03754), 1895–1962 of synapsin IIa cDNA (M27925), 565–662 of syntaxin 1B cDNA (M95735) and 1051–1121 of α-tubulin cDNA (BC060572).

Quantitative real-time PCR was performed using ABI Prism 7700 (Applied Biosystems) employing a three step cycling protocol (denaturation/annealing/extension). Ten microlitres of diluted cDNA was amplified with Platinum Quantitative PCRMix-UDG (Invitrogen) according to manufacturer's instructions for multiplex real-time PCR, in the presence of ROX reference dye. The no-template negative control was routinely run in every PCR. Samples were subjected to real-time PCR amplification of the target mRNA (100 nm FAM-labelled primer) and alpha-tubulin (50 nm JOE-labelled primer). The reactions were incubated at 50 °C for 2 min to activate uracil *N*′-glycosylase for PCR carryover decontamination, and then at 95 °C for 2 min for template denaturation and hot start prior to PCR cycling. A cycling protocol consisted of three stages: 15 s at 95 °C for denaturation; 30 s at 55 °C for annealing and 30 s at 72 °C for extension. Thirty-five to 40 cycles were required for quantification of the specific amplicons studied. After the final cycle of the PCR, a melt curve analysis was routinely performed. The reactions were cooled to 60 °C and then heated up to 90 °C to denature double-strand PCR products. The fluorescent signal recorded during DNA melting was plotted against temperature to generate the melt curve (d*F*/d*T*) for each reaction. Quantification was performed using the cycle threshold (Ct) method and results are presented as percentage of control. Data were analysed using ANOVA followed by *posthoc* test using StatView software, and presented as the mean ± SEM.

Western blot

Crude plasma membranes were prepared from each rat lumbar spinal cord as described previously (Nicot *et al*., 2003). Two micrograms of total protein was loaded on a 3–8% polyacrylamide Tris-acetate gel (Invitrogen). Electrophoresis was performed for 60 min at 150 V on ice. The proteins were then transferred onto a polyvinylidene difluoride (PVDF) membrane for 60 min at 30 V using Invitrogen semi-dry transfer procedure. Immunodetection was performed using anti-PMCA2 (1 : 5000, rabbit polyclonal; Research Diagnostic, Flanders, NJ, USA), anti-synapsin IIa (1 : 10 000, mouse monoclonal; BD Pharmingen, Palo Alto, USA), anti-syntaxin 1B (1 : 10 000; rabbit polyclonal; Synaptic Systems, Goettingen, Germany) or anti-α-tubulin (1 : 40 000, mouse monoclonal; Sigma-Aldrich, St-Louis, MO, USA). Secondary antibodies coupled to horseradish peroxidase were used at indicated concentrations (anti-rabbit, 1 : 10 000; anti-mouse 1 : 20 000–40 000; Chemicon, Temecula, CA, USA). Signal was visualized using ECL Plus kit (Amersham Pharmacia Biotech; Piscataway, NJ, USA) after exposure of blots to Hyperfilm ECL (Amersham Pharmacia Biotech, Piscataway, USA) for 30–180 s and quantified using the Un-Scan-It software (Silk Scientific, Orem, UT, USA). Results are presented as percentage of control after normalization to alpha-tubulin.

Spinal cords obtained from mice were homogenized in 200 μL lysis buffer consisting of 50 mM Tris, 150 mM NaCl, 0.02%, sodium azide, 0.1% sodium dodecylsulphate, 1% NP40, 0.5% deoxycholic acid, 2mM PMSF, 2 μg/mL leupeptin, 2 μg/mL aprotinin, 2 μg/mL pepstatin, at 4 °C. After 20 min centrifugation at 14 000 × ***g*** at 4 °C, supernatants were collected and frozen at −20 °C for further analysis. Total protein (10 μg) was loaded on a 7% Tris-Gly gel. The rest of the procedure was performed as described above.

Immunocytochemistry

Control and EAE mice on day 24 PI (clinical score 3, $n = 3$) were anaesthetized using a lethal dose of pentobarbital and perfused with saline followed by 4% formaldehyde in phosphate buffer (0.1 M). Lumbar spinal cords were postfixed for 3 h, cryoprotected in 20% sucrose and frozen on dry ice. Cryostat sections were used for histological analysis of CD4 (LT3T4), Mac-1 (CD11b/CD18), PMCA2 and 4′,6-diamidino-2-phenylindole (DAPI) staining. Tissue sections collected from control and EAE mice were stained simultaneously. Ten-micrometer-thick sections mounted on Superfrost plus slides or 40-μm-thick free-floating sections were treated with 3% H_2O_2 in phosphate buffer for 30 min followed by 30% normal goat serum, 0.05%

Triton X-100, PBS for 30 min. They were then incubated overnight with PMCA2 antibody diluted 1 : 2000 in 3% normal goat serum and 0.05% Triton X-100, at 4 °C. The sections were then washed for 45 min in phosphate buffer followed by incubation with biotinylated secondary antibody (Jackson Immuno-Research, West Grove, PA, USA; 1 : 200 dilution) for 45 min. Sections were incubated with streptavidin-peroxidase complex (Perkin-Elmer Life Sciences, Boston, MA) at 1 : 200 for 1 h, rinsed, and incubated with tyramide-fluorescein solution (TSA, PerkinElmer Life Sciences; 1 : 100 dilution) for 5–10 min at room temperature. For identification of lymphocytes and macrophages/microglia, CD4 (LT3T4, BD Pharmingen, San Diego, CA, USA) and Mac-1 (CD11b/CD18; BD Pharmingen) rat monoclonal antibodies were used at 1 : 100 and 1 : 200 dilution, respectively. After overnight incubation at 4 °C, sections were rinsed and incubated 1 h at room temperature with FITC- or Texas Red-coupled rat antibodies (1 : 200), followed by PBS rinses for 1 h. The sections were air-dried and coverslipped with Vectashield or Vectashield-DAPI (Vector labs). Negative controls were treated as described above except that primary antibodies were omitted.

Image analysis

To quantify PMCA2 immunostaining, images were captured under a fluorescent microscope (×200) using the image software and an Olympus D50 digital camera. Same light intensity and exposure time were applied to all photographs for each staining. Pictures in the ventral grey matter were collected from the two sides of three sections per animal. All images were then analysed with PhotoShop with a 300-μm square box area being measured, averaged, and compared among different animals. A *t*-test was applied to examine the statistical significance ($P < 0.05$) of differences in mean values between control and EAE samples.

Results

A number of neuronal genes are differentially expressed at onset of acute EAE in the Lewis rat (Nicot *et al*., 2003). Among those are PMCA2, synapsin IIa and syntaxin 1B whose expression is dramatically reduced at the earliest clinical stage. The present study assessed the expression of the aforementioned genes during the entire course of the disease in two different EAE models.

Assessment of real-time PCR method

We took advantage of the recent Lux primer multiplex real-time PCR method to analyse the relative expression levels of PMCA2, synapsin IIa and syntaxin 1B. This approach enabled the measurement of mRNA levels in individual lumbar spinal cords, not only in the rat, but also in the mouse, which yields limited amounts of tissue. Quantitative real-time PCR using fluorogenic LUX primers has been developed recently and used for the quantification of transcript levels of multiple genes in the same sample (Lowe *et al*., 2003; Di Giovanni *et al*., 2005). Therefore, we performed several control experiments to validate this method in our hands. To assess the specificity of each PCR, we generated the melt curve (dF/dT) by plotting the fluorescent signal recorded during DNA melting against the temperature at the end of each reaction. The respective *T*m, indicated by the peak of the curve, was 85 °C for the PMCA2 amplicon, 82 °C for synapsin IIa or syntaxin 1B, and 82.5–83 °C for α-tubulin (Fig. 1A). No specific product was obtained from the RNA sample (no reverse transcriptase). The non-specific products, which result from primer-dimer formation, were detectable only when PCR was performed for 45 cycles and displayed lower *T*m (70–75 °C) than that of specific amplicons (data not shown). Hence, the amplification specificity in each reaction was confirmed by the presence of a correct specific *T*m and by the absence of a lower non-specific *T*m.

Quantification of transcript levels in control and EAE samples was achieved by measuring the cycle threshold (Ct) for target gene and α-tubulin for each cDNA using the ABI Prism 7700

software (Applied Biosystems). The parameter Ct is defined as the first cycle in which there is a significant elevation in fluorescence above the threshold. To assess amplification efficiencies of target gene and alpha-tubulin, relative standard curves were generated with serial dilutions of total cDNA (300 ng to 1.5 ng). As indicated in Fig. 1B, the differences between target and tubulin transcript amplification efficiencies (indicated by the slope of the standard curves) were lower than 0.4. As amplification efficiencies of target and α-tubulin transcripts were similar, analysis of relative expression could be performed using the 2-ΔΔCt method (see Livak & Schmittgen, 2001).

Restitution of PMCA2 levels precedes functional recovery from acute EAE in the Lewis rat

To determine the correlation between PMCA2 expression and manifestation of neurological symptoms, we used real-time PCR and quantified transcript levels of the calcium pump in the lumbar spinal cord of Lewis rats during the various clinical phases of acute EAE including recovery. MBP-inoculated rats developed progressive symptoms starting on day 11 post-immunization (PI), manifested hindlimb paralysis between days 13 and 14, begun to remit on day 15 PI and completely recovered by day 18 PI (Fig. 2A). PMCA2 transcript levels were 46% of controls at onset of symptoms on day 11 PI, continued to decrease subsequently reaching the lowest levels (30%) by day 13 PI. However, on day 14 PI, immediately before the initiation of remission, PMCA2 expression increased to 61% of controls and remained at the same level after complete recovery on day 18 PI. Although PMCA2 mRNA levels on days 14 and 18 PI were still lower in diseased as compared to control rats, statistical analysis indicated that the results were not significantly different (Fig. 2B). To determine whether PMCA2 protein expression follows the same pattern, we performed western blot analysis using lumbar spinal cord crude membrane extracts. In agreement with the results obtained by real-time PCR, we found that PMCA2 protein levels were significantly decreased on days 11 through 13 and returned to control values by day 14 PI (Fig. 2C).

The PMCA gene family encodes four isoforms (PMCA1–4) (Shull & Greeb, 1988; Verma *et al.*, 1988; Greeb & Shull, 1989; Strehler, 1990; Keeton & Shull, 1995). To determine whether the changes observed are unique to PMCA isoform 2, we quantified transcript levels of the other isoforms (PMCA1, 3 and 4) by semi-quantitative RT-PCR using primers specific for each isoform. These studies were performed on rats at stage E3 (day 13 PI) as PMCA2 expression is the lowest at this phase as indicated both by semi-quantitative RT-PCR (Nicot *et al.*, 2003) and real-time PCR (Fig. 2B). PMCA1, 3 and 4 transcript levels in the lumbar spinal cord were not different than controls (Table 1) indicating that changes in the expression of PMCA2 are selective and specific to this isoform.

Synapsin IIa and syntaxin 1B expression is differentially modulated during MBP-induced acute EAE in the Lewis rat

To determine expression patterns of the synaptic/vesicular proteins synapsin IIa and syntaxin 1B during the entire course of EAE in the Lewis rat, we performed real-time PCR at different days following immunization including the phases when gradual remission occurs. As expected, expression of synapsin IIa decreased at onset of symptoms (day 11 PI, 53% of control), and reached the lowest level on day 13 PI (31%) (Fig. 3A). Thereafter, synapsin IIa expression started to recover. Although transcript levels had a tendency to remain low (62% and 73% on days 14 and 18 PI, respectively), the values were not significantly different from controls (Fig. 3A). Immunoblot analysis of membrane extracts indicated that synapsin IIa protein levels were also significantly decreased on day 12 PI, 24 h after the first reduction in mRNA levels is detected (Fig. 3B). Synapsin IIa levels remained low on day 13 PI and were restored to control values on day 14 PI, immediately before the onset of remission from clinical symptoms.

In contrast, analysis of syntaxin 1B mRNA and protein levels raised the possibility of post-transcriptional regulation during recovery. Although syntaxin 1B mRNA levels were already decreased on day 11 PI (52% of control, Fig. 4A), protein levels appeared to be more stable as they were not statistically different from controls even on days 11 and 12 PI (Fig. 4B). Moreover, whereas syntaxin 1B transcript levels remained low despite complete remission on day 18 PI (Fig. 4A), protein levels were quickly restored to control values after a brief decrease on day 13 PI. The restitution of syntaxin 1B protein levels in spite of reduced mRNA on days 14 and 18 PI suggests post-transcriptional regulation, an attempt to restore normal synaptic function.

PMCA2, synapsin IIa and syntaxin 1B expression is decreased during the clinical course of MOG-induced EAE in the mouse

To determine whether the molecular changes observed in acute EAE in the rat also occur in a different EAE model, we quantified PMCA2, synapsin IIa and syntaxin 1B transcript levels in the lumbar spinal cord of C57Bl/6 mice during the course of the disease starting at onset of symptoms. C57Bl/6 mice exhibit their first deficits (tail weakness) on day 13 PI, reach the highest clinical score by day 16 PI and remain affected thereafter for several weeks. In agreement with our findings in the rat, PMCA2 transcript levels decreased at onset of neurological deficits (55% of control on day 14 PI, clinical score 1, Fig. 5), were further reduced on subsequent days (39 and 36% of control on days 15 and 16 PI) and remained low at 24 day PI (35% of control). Similarly, synapsin IIa and syntaxin 1B expression was 56 and 66% of control, respectively, at onset of symptoms (Fig. 5). Syntaxin 1B mRNA levels remained diminished throughout the course of the disease, whereas synapsin IIa expression was lower than controls until day 16 PI (Fig. 5). Immunoblot analysis confirmed that PMCA2 and synapsin IIa protein levels were markedly reduced in the spinal cord during EAE (Fig. 6). As in the case of acute EAE in the rat, syntaxin 1B protein levels (Fig. 6) remained stable and did not show a significant modulation ($P = 0.07$).

Inflammatory cell infiltration and reduction in PMCA2 immunoreactivity correlate in MOG-induced EAE in C57Bl6 mice

To establish a potential correlation between inflammatory cell infiltration and alterations in PMCA2 protein expression, we performed immunocytochemistry on spinal cord sections using antibodies against PMCA2 and markers of T-cells (CD4) and macrophages/microglia (Mac-1). We defined the general inflammatory infiltration and microglial activation in the spinal cord of control and EAE mice using DAPI, CD4 and Mac-1 antibodies. DAPI staining revealed dense cell infiltration in the white matter and around blood vessels (Fig. 7A–C). CD4 immunoreactive lymphocytes were mostly localized to the dorsal and ventral funiculi, though they could also be found in other regions of the white matter in mice affected by EAE (Fig. 7D–G). Scarce CD4 positive cells were observed in the grey matter of EAE animals (data not shown). In contrast, CD4 immunoreactive lymphocytes were not found in the CNS parenchyma of controls. Analysis of PMCA2 immunoreactivity indicated strongly labelled axon bundles in control spinal cords (Fig. 7K and M), whereas the staining was greatly reduced in EAE (Fig. 7L and N).

Distribution of Mac-1 immunoreactivity, a marker of monocytic lineage cells including macrophages and microglia, indicated light staining in the grey matter of controls (Fig. 8A), especially in cells exhibiting the morphology of resting microglia (not shown). In contrast, numerous, strongly stained Mac-1 positive cells were observed throughout the white and grey matter of the spinal cord of EAE animals (Fig. 8B).

Labelling with PMCA2 antibody revealed strong, punctate staining throughout the grey matter (Fig. 8C). Moreover, the plasma membrane of numerous neurons was clearly stained (Fig. 8E–

F). PMCA2 immunoreactivity was greatly reduced in EAE animals (Fig. 8D). Quantification of the fluorescent signal confirmed the reduction in PMCA2 staining in spinal cord grey matter of EAE animals as compared to controls (relative optical densities; control mice 15.0 ± 0.5, $n = 3$, EAE mice 8.4 ± 0.8, $n = 3$; $P < 0.05$).

Discussion

Our present study clearly establishes an inverse correlation between the expression pattern of the neuronal calcium pump PMCA2 and the course of symptomatic disease in two different EAE models. Moreover, we report that two synaptic proteins may also play a role in neuronal dysfunction during the early disease phases in both models whereas their contributions may diverge at later stages. Interestingly, among the three proteins, PMCA2 expression was the earliest to be affected and to recover during the course of EAE, supporting a key role for this protein in neuronal dysfunction, as suggested by our *in vitro* studies on spinal cord neurons (Kurnellas *et al.*, 2005).

The manifestation of chronic EAE in the C57Bl/6 mouse and acute EAE in the Lewis rat differ substantially in clinical course as well as pathohistology. Demyelination is little or absent in the MBP-inoculated Lewis rat but extensive in the MOG-immunized C57Bl/6 mouse. Thus, our findings suggest that at least some of the molecular changes that underlie neuronal dysfunction are not the direct result of demyelination, but may be the consequence of inflammation. The reduction in the expression of other synaptic/membrane proteins such as MAP2, synaptophysin, synapsin I and PSD-95 in the rat acute model (Zhu *et al.*, 2003) also support inflammation-mediated neuronal dysfunction during EAE. Moreover, in a different animal model of MS induced by injection of a murine Theiler's virus substrain GDVII, severe axonal pathology in normal appearing white matter has been shown to occur in the absence of apparent demyelination. Furthermore, loss of myelin can be observed subsequent to axonal pathology leading to the hypothesis that axonal injury may be a trigger for demyelination (Tsunoda *et al.*, 2003). Thus, the present investigations highlight additional molecular players of axonal dysfunction that are common to both acute, remitting and chronic non-remitting EAE and shed light onto the temporal course of events that may contribute to neuronal and axonal pathology in the disease.

Axonal damage during MS, although recognized in early studies, has recently received increasing attention (Charcot, 1868; Dawson, 1916; reviewed in Ferguson *et al.*, 1997; Trapp *et al.*, 1998, [1999]; Compston, 1999; De Stefano *et al.*, 1999; Bitsch *et al.*, 2000; Bjartmar & Trapp, 2001; Bjartmar *et al.*, 2001; Peterson *et al.*, 2001). Although axonal transection and loss was considered to be a correlate of permanent disability during the late stages of MS, axonal pathology is now observed at the earliest clinical phases of the disease (Trapp *et al.*, 1998; Matthews *et al.*, 1998; Kuhlmann *et al.*, 2002; Filippi *et al.*, 2003). Moreover, several investigations indicate that neuronal/axonal dysfunction and damage may be reversible. MRS studies demonstrate a transient decrease in the neuronal marker *N*-acetyl aspartate during acute relapses of MS (Davie *et al.*, 1994). In addition, axonal anomalies such as accumulation of amyloid precursor protein (APP) and dephosphorylation of neurofilament H, are not accompanied by ultrastructural changes reflecting axonal transection such as formation of terminal ovoids and swellings. This raises the possibility that axonal dysfunction does not always lead to axonal transection and may be reversible (Mancardi *et al.*, 2001). Moreover, axonal pathology can be also demonstrated in normally myelinated white matter of MS brain, as assessed for example by abnormal ubiquitination of axons (Giordana *et al.*, 2002). Interestingly, serotoninergic transmission, which is interrupted during the initial paralytic stages of EAE due to damage of bulbospinal neurons, is re-established during remission (Sandyk, 1999) and nerve conduction in the peripheral and central nervous system is restored during recovery from acute EAE in the Lewis rat (Pender, 1989). Although this later

improvement was attributed to partial remyelination of fibers, amelioration of symptoms due to the reversal of aberrant neuronal gene expression during remission can not be ruled out. Our findings further emphasize this notion, as the decrease in PMCA2 transcript levels is reversed just before the initiation of recovery, suggesting that restoration of PMCA2 levels is necessary for reinstating normal neuronal function. Similarly, synapsin IIa protein expression returned to control values during remission. Whereas transcript levels of syntaxin 1B, which is exclusively localized to grey matter (Aguado *et al.*, 1999), remained low in the Lewis rat despite clinical recovery, protein levels remained stable for a longer period, decreased and finally tended to return to control values. Our results are in conceptual agreement with the studies of Zhu *et al.* (2003) showing a partial recovery of some other dendritic and synaptic proteins during remission. Therefore, reversible mechanisms underlying axonal/neuronal pathology at early stages of MS or EAE may be different from those mediating axonal transection and loss at later phases.

It should be emphasized that clinical scores reflect changes only in motor function and do not account for other impairments such as sensory alterations. Indeed, the dorsal horn of the spinal cord, a region primarily involved in nociception, is also affected by inflammation during EAE. However, due to the difficulty in assessing pain in EAE animals, few experimental data exist in affected rodents. So far, Pender (1986) has shown that hypoalgesia to mechanical stimulus resolves before motor deficits in rats. Aicher *et al.* (2004) have reported that thermal hypoalgesia appears just before motor deficits, while mild thermal hyperalgesia occurs during the chronic phase of MOG-induced EAE in mice. Whether the reduction in the expression of proteins in the dorsal horn such as PMCA2, synapsin or syntaxin 1B contribute to some nociceptive alterations needs to be further addressed.

A reduction in calcium extrusion may be of particular significance for axonal pathology because an increase in intra-axonal calcium is an important trigger causing injury in several disorders (Ransom *et al.*, 1990; George *et al.*, 1995). Interestingly, the importance of neuronal PMCA activity in maintaining intracellular calcium balance has been recently highlighted (Pottorf & Thayer, 2002). We also found that blockade of PMCA2 in spinal cord neuronal cultures results in damage of processes, similar to that observed in multiple sclerosis, followed by cell death (Kurnellas *et al.*, 2005). *In vivo*, such pathological changes may activate compensatory mechanisms to protect cells or limit the extent of the injury. To this end, the suppression of PMCA2-mediated calcium extrusion could be compensated by an increase in the levels and activity of other PMCA isoforms to maintain calcium homeostasis and prevent the induction of neuronal injury cascades. However, such compensatory mechanisms do not appear to occur during EAE. Indeed, whereas PMCA2 mRNA levels in the rat spinal cord dropped to their lowest value at the peak of the disease, transcript levels of PMCA1, 3 and 4 were not significantly different from controls, indicating selective regulation of PMCA2 expression. This specific down-regulation also occurs after spinal cord injury (Elkabes & Nicot, 2003; Tachibana *et al.*, 2004). Interestingly, the specialized and non-redundant role of PMCA2 is indicated by the phenotype of mice with mutations in the PMCA2 gene. Deafness, unsteady gait and unbalanced movement, impairment of calcium transport into milk, and partial loss of motor neurons in the spinal cord are the major anomalies reported to date (Kozel *et al.*, 1998; Street *et al.*, 1998; Shull, 2000; Kurnellas *et al.*, 2005; Reinhardt *et al.*, 2004). Thus, the presence of other isoforms does not compensate for the absence or reduced PMCA2 activity.

Taken together, our results pinpoint the down-regulation of a protein involved in calcium extrusion as a potential important contributor to neuronal pathology in EAE. The reduction in PMCA2 may affect calcium homeostasis leading to induction of injury cascades. Recent studies have also indicated aberrance in other calcium-related mechanisms during EAE. Kornek *et al.* (2000, 2001) reported abnormal localization and integration of N-type calcium channels in dystrophic axons suggesting aberrant calcium influx. Altered axonal expression of

sodium channels and Na^+ / Ca^{2+} exchanger has been suggested as a mechanism of axonal damage in EAE and MS (Nicot *et al.*, 2003; Craner *et al.*, 2003, 2004). It is worth noting that, among proteins involved in ion homeostasis, PMCA2 expression is reduced at the very first manifestation of clinical EAE and is well correlated with the disease course. Finally, increased calcium not only induces injury mechanisms but also interferes with synaptic communication. In addition, defects in proteins involved in vesicular and synaptic function can further exacerbate abnormal synaptic transmission by disrupting neurotransmitter release. In conclusion, our studies and those of others suggest a potential role for abnormal ion homeostasis and synaptic/vesicular function in axonal/neuronal damage during EAE. These anomalies may indeed interfere with normal synaptic transmission and neuron–glia interactions, increasing the vulnerability of neurons to injury due to impediments in myelin or glia-mediated trophic support. By shedding light on molecular mechanisms of neuronal damage during neuroinflammatory diseases, the present and other ongoing studies are of pivotal importance to advance our knowledge of MS pathogenesis. They further support the need of combinatory therapeutic strategies including those aimed at neuroprotection in neuroinflammatory diseases such as MS (Giuliani & Yong, 2003; Brand-Schieber & Werner, 2004; Kanwar *et al.*, 2004).

Acknowledgments

We are grateful to Patricia Mechighel for technical help and Dr Patrick Kitabgi for his support. A.N. was the recipient of a postdoctoral fellowship (candidat Inserm) from Fondation de la Recherche Médicale. This work was supported by Grant NS 046363 (NIH/NINDS) to S.E and funds from INSERM to U732.

Abbreviations

Ct	cycle threshold
DAPI	4′,6-diamidino-2-phenylindole
EAE	experimental autoimmune encephalomyelitis
MOG	myelin oligodendrocyte glycoprotein
MBP	myelin basic protein
MS	multiple sclerosis
PMCA2	plasma membrane calcium ATPase 2
PI	post-immunization
RT	reverse transcriptase

References

Aguado F, Majo G, Ruiz-Montasell B, Llorens J, Marsal J, Blasi J. Syntaxin 1A and 1B display distinct distribution patterns in the rat peripheral nervous system. Neuroscience 1999;88:437–446. [PubMed: 10197765]

Ahmed Z, Gveric D, Pryce G, Baker D, Leonard JP, Cuzner ML, Diemel LT. Myelin/axonal pathology in interleukin-12 induced serial relapses of experimental allergic encephalomyelitis in the Lewis rat. Am. J. Pathol 2001;158:2127–2138. [PubMed: 11395390]

Aicher SA, Silverman MB, Winkler CW, Bebo BF Jr. Hyperalgesia in an animal model of multiple sclerosis. Pain 2004;110:560–570. [PubMed: 15288396]

Bitsch A, Schuchardt J, Bunkowski S, Kuhlmann T, Bruck W. Acute axonal injury in multiple sclerosis. Correlation with demyelination and inflammation. Brain 2000;123:1174–1183. [PubMed: 10825356]

Bjartmar C, Kinkel RP, Kidd G, Rudick RA, Trapp BD. Axonal loss in normal-appearing white matter in a patient with acute MS. Neurology 2001;57:1248–1252. [PubMed: 11591844]

Bjartmar C, Trapp BD. Axonal and neuronal degeneration in multiple sclerosis: mechanisms and functional consequences. Curr. Opin. Neurol 2001;14:271–278. [PubMed: 11371748]

Brand-Schieber E, Werner P. Calcium channel blockers ameliorate disease in a mouse model of multiple sclerosis. Exp. Neurol 2004;189:5–9. [PubMed: 15296830]

Charcot JM. Histologie de la sclérose en plaques. Gaz. Hop. Civils Militaires 1868;140:141 557–141 558.

Compston A. The pathological anatomy of the lesion in multiple sclerosis. Brain Res. Bull 1999;50:463–464. [PubMed: 10643485]

Craner MJ, Kataoka Y, Lo AC, Black JA, Baker D, Waxman SG. Temporal course of upregulation of Na(v)1.8 in Purkinje neurons parallels the progression of clinical deficit in experimental allergic encephalomyelitis. J. Neuropathol. Exp. Neurol 2003;62:968–975. [PubMed: 14533785]

Craner MJ, Newcombe J, Black JA, Hartle C, Cuzner ML, Waxman SG. Molecular changes in neurons in multiple sclerosis: altered axonal expression of Nav1.2 and Nav1.6 sodium channels and Na^+ / Ca^{2+} exchanger. Proc. Natl Acad. Sci. USA 2004;101:8168–8173. [PubMed: 15148385]

Davie CA, Hawkins CP, Barker GJ, Brennan A, Tofts PS, Miller DH, McDonald WI. Serial proton magnetic resonance spectroscopy in acute multiple sclerosis lesions. Brain 1994;117:49–58. [PubMed: 8149214]

Dawson JW. The histology of disseminated sclerosis. Trans. Royal. Soc. Edin 1916;50:517–540.

De Stefano N, Narayanan S, Matthews PM, Francis GS, Antel JP, Arnold DL. *In vivo* evidence for axonal dysfunction remote from focal cerebral demyelination of the type seen in multiple sclerosis. Brain 1999;122:1933–1939. [PubMed: 10506094]

Di Giovanni S, De Biase A, Yakovlev A, Finn T, Beers J, Hoffman EP, Faden AI. *In vivo* and *in vitro* characterization of novel neuronal plasticity factors identified following spinal cord injury. J. Biol. Chem 2005;280:2084–2091. [PubMed: 15522871]

Elkabes S, Nicot A. Aberrant calcium extrusion mechanisms may contribute to secondary spinal cord injury. J. Neurol 2003;250:179. [PubMed: 12574948]

Ferguson B, Matyszak MK, Esiri MM, Perry VH. Axonal damage in acute multiple sclerosis lesions. Brain 1997;120:393–399. [PubMed: 9126051]

Filippi M, Bozzali M, Rovaris M, Gonen O, Kesavadas C, Ghezzi A, Martinelli V, Grossman RI, Scotti G, Comi G, Falini A. Evidence for widespread axonal damage at the earliest clinical stage of multiple sclerosis. Brain 2003;126:433–437. [PubMed: 12538409]

Fresu L, Dehpour A, Genazzani AA, Carafoli E, Guerini D. Plasma membrane calcium ATPase isoforms in astrocytes. Glia 1999;28:150–155. [PubMed: 10533058]

Garcia ML, Strehler EE. Plasma membrane calcium ATPases as critical regulators of calcium homeostasis during neuronal cell function. Front. Biosci 1999;4:D869–D882. [PubMed: 10577388]

George EB, Glass JD, Griffin JW. Axotomy-induced axonal degeneration is mediated by calcium influx through ion-specific channels. J. Neurosci 1995;15:6445–6452. [PubMed: 7472407]

Giordana MT, Richiardi P, Trevisan E, Boghi A, Palmucci L. Abnormal ubiquitination of axons in normally myelinated white matter in multiple sclerosis brain. Neuropathol. Appl. Neurobiol 2002;28:35–41. [PubMed: 11849561]

Giuliani F, Yong VW. Immune-mediated neurodegeneration and neuroprotection in MS. Int. MS J 2003;10:122–130. [PubMed: 14977489]

van der Goes A. Models for demyelination. Prog. Brain Res 2001;132:146–163.

Greeb J, Shull GE. Molecular cloning of a third isoform of the calmodulin-sensitive plasma membrane Ca^{2+}-transporting ATPase that is expressed predominantly in brain and skeletal muscle. J. Biol. Chem 1989;264:18569–18576. [PubMed: 2530223]

Hilfiker S, Pieribone VA, Czernik AJ, Kao HT, Augustine GJ, Greengard P. Synapsins as regulators of neurotransmitter release. Philos. Trans. R. Soc. Lond. B Biol. Sci 1999;354:269–279. [PubMed: 10212475]

Imrich H, Harzer K. On the role of peripheral macrophages during active experimental allergic encephalomyelitis (EAE). J. Neural. Transm 2001;108:379–395. [PubMed: 11475006]

Kanwar JR, Kanwar RK, Krissansen GW. Simultaneous neuroprotection and blockade of inflammation reverses autoimmune encephalomyelitis. Brain 2004;127:1313–1331. [PubMed: 15130951]

Keeton TP, Shull GE. Primary structure of rat plasma membrane Ca(2+)-ATPase isoform 4 and analysis of alternative splicing patterns at splice site A. Biochem. J 1995;306:779–785. [PubMed: 7702574]

Kornek B, Storch MK, Bauer J, Djamshidian A, Weissert R, Wallstroem E, Stefferl A, Zimprich F, Olsson T, Linington C, Schmidbauer M, Lassmann H. Distribution of a calcium channel subunit in dystrophic axons in multiple sclerosis and experimental autoimmune encephalomyelitis. Brain 2001;124:1114–1124. [PubMed: 11353727]

Kornek B, Storch MK, Weissert R, Wallstroem E, Stefferl A, Olsson T, Linington C, Schmidbauer M, Lassmann H. Multiple sclerosis and chronic autoimmune encephalomyelitis: a comparative quantitative study of axonal injury in active, inactive, and remyelinated lesions. Am. J. Pathol 2000;157:267–276. [PubMed: 10880396]

Kozel PJ, Friedman RA, Erway LC, Yamoah EN, Liu LH, Riddle T, Duffy JJ, Doetschman T, Miller ML, Cardell EL, Shull GE. Balance and hearing deficits in mice with a null mutation in the gene encoding plasma membrane Ca^{2+}-ATPase isoform 2. J. Biol. Chem 1998;273:18693–18696. [PubMed: 9668038]

Kuhlmann T, Lingfeld G, Bitsch A, Schuchardt J, Bruck W. Acute axonal damage in multiple sclerosis is most extensive in early disease stages and decreases over time. Brain 2002;125:2202–2212. [PubMed: 12244078]

Kurnellas MP, Nicot A, Shull GE, Elkabes S. Plasma membrane calcium ATPase deficiency causes neuronal pathology in the spinal cord: a potential mechanism for neurodegeneration in multiple sclerosis and spinal cord injury. FASEB J 2005;19:298–300. [PubMed: 15576480]

Lin RC, Scheller RH. Mechanisms of synaptic vesicle exocytosis. Annu. Rev. Cell Dev. Biol 2000;16:19–49. [PubMed: 11031229]

Livak KJ, Schmittgen TD. Analysis of relative gene expression data using real-time quantitative PCR and the 2(-Delta Delta C(T) method. Methods 2001;25:402–408. [PubMed: 11846609]

Lowe B, Avila HA, Bloom FR, Gleeson M, Kusser W. Quantitation of gene expression in neural precursors by reverse-transcription polymerase chain reaction using self-quenched, fluorogenic primers. Anal. Biochem 2003;315:95–105. [PubMed: 12672417]

Mancardi G, Hart B, Roccatagliata L, Brok H, Giunti D, Bontrop R, Massacesi L, Capello E, Uccelli A. Demyelination and axonal damage in a non-human primate model of multiple sclerosis. J. Neurol. Sci 2001;184:41–49. [PubMed: 11231031]

Matthews PM, De Stefano N, Narayanan S, Francis GS, Wolinsky JS, Antel JP, Arnold DL. Putting magnetic resonance spectroscopy studies in context: axonal damage and disability in multiple sclerosis. Semin. Neurol 1998;18:327–336. [PubMed: 9817537]

Nicot A, Ratnakar PV, Ron Y, Chen CC, Elkabes S. Regulation of gene expression in experimental autoimmune encephalomyelitis indicates early neuronal dysfunction. Brain 2003;126:398–412. [PubMed: 12538406]

Pender MP. Ascending impairment of nociception in rats with experimental allergic encephalomyelitis. J. Neurol. Sci 1986;75:317–328. [PubMed: 3490542]

Pender MP. Recovery from acute experimental allergic encephalomyelitis in the Lewis rat. Early restoration of nerve conduction and repair by Schwann cells and oligodendrocytes. Brain 1989;112:393–416. [PubMed: 2468391]

Pendlebury ST, Lee MA, Blamire AM, Styles P, Matthews PM. Correlating magnetic resonance imaging markers of axonal injury and demyelination in motor impairment secondary to stroke and multiple sclerosis. Magn. Reson. Imaging 2000;18:369–378. [PubMed: 10788713]

Peterson JW, Bo L, Mork S, Chang A, Trapp BD. Transected neurites, apoptotic neurons, and reduced inflammation in cortical multiple sclerosis lesions. Ann. Neurol 2001;50:389–400. [PubMed: 11558796]

Pitt D, Werner P, Raine CS. Glutamate excitotoxicity in a model of multiple sclerosis. Nature Med 2000;6:67–70. [PubMed: 10613826]

Pottorf WJ, Thayer SA. Transient rise in intracellular calcium produces a long-lasting increase in plasma membrane calcium pump activity in rat sensory neurons. J. Neurochem 2002;83:1002–1008. [PubMed: 12421373]

Ransom BR, Stys PK, Waxman SG. The pathophysiology of anoxic injury in central nervous system white matter. Stroke 1990;21:III52–III57. [PubMed: 2237986]

Reinhardt TA, Lippolis JD, Shull GE, Horst RL. Null mutation in the gene encoding plasma membrane Ca^{2+}-ATPase isoform 2 impairs calcium transport into milk. J. Biol. Chem 2004;279:42369–42373. [PubMed: 15302868]

Rosahl TW, Spillane D, Missler M, Herz J, Selig DK, Wolff JR, Hammer RE, Malenka RC, Sudhof TC. Essential functions of synapsins I and II in synaptic vesicle regulation. Nature 1995;375:488–493. [PubMed: 7777057]

Sandyk R. Serotonergic neuronal sprouting as a potential mechanism of recovery in multiple sclerosis. Int. J. Neurosci 1999;97:131–138. [PubMed: 10681122]

Shull GE. Gene knockout studies of Ca^{2+}-transporting ATPases. Eur. J. Biochem 2000;267:5284–5290. [PubMed: 10951186]

Shull GE, Greeb J. Molecular cloning of two isoforms of the plasma membrane Ca^{2+}-transporting ATPase from rat brain. Structural and functional domains exhibit similarity to Na^{+},K^{+}- and other cation transport ATPases. J. Biol. Chem 1988;263:8646–8657. [PubMed: 2837461]

Smith T, Groom A, Zhu B, Turski L. Autoimmune encephalomyelitis ameliorated by AMPA antagonists. Nature Med 2000;6:62–66. [PubMed: 10613825]

Stauffer TP, Hilfiker H, Carafoli E, Strehler EE. Quantitative analysis of alternative splicing options of human plasma membrane calcium pump genes. J. Biol. Chem 1993;268:25993–26003. [PubMed: 8245032]

Storch MK, Weissert R, Steffer A, Birnbacher R, Wallstrom E, Dahlman I, Ostensson CG, Linington C, Olsson T, Lassmann H. MHC gene related effects on microglia and macrophages in experimental autoimmune encephalomyelitis determine the extent of axonal injury. Brain Pathol 2002;12:287–299. [PubMed: 12146797]

Street VA, McKee-Johnson JW, Fonseca RC, Tempel BL, Noben-Trauth K. Mutations in a plasma membrane Ca^{2+}-ATPase gene cause deafness in deafwaddler mice. Nature Genet 1998;19:390–394. [PubMed: 9697703]

Strehler EE. Plasma membrane Ca^{2+} pumps and Na^{+}/Ca^{2+} exchangers. Semin. Cell Biol 1990;1:283–295. [PubMed: 2151738]

Tachibana T, Ogura H, Tokunaga A, Dai Y, Yamanaka H, Seino D, Noguchi K. Plasma membrane calcium ATPase expression in the rat spinal cord. Mol. Brain Res 2004;131:26–32. [PubMed: 15530649]

Trapp BD, Peterson J, Ransohoff RM, Rudick R, Mork S, Bo L. Axonal transection in the lesions of multiple sclerosis. N. Engl. J. Med 1998;338:278–285. [PubMed: 9445407]

Trapp BD, Ransohoff R, Rudick R. Axonal pathology in multiple sclerosis: relationship to neurologic disability. Curr. Opin. Neurol 1999;12:295–302. [PubMed: 10499174]

Tsunoda I, Kuang LQ, Libbey JE, Fujinami RS. Axonal injury heralds virus-induced demyelination. Am. J. Pathol 2003;162:1259–1269. [PubMed: 12651618]

Verma AK, Filoteo AG, Stanford DR, Wieben ED, Penniston JT, Strehler EE, Fischer R, Heim R, Vogel G, Mathews S. Complete primary structure of a human plasma membrane Ca^{2+} pump. J. Biol. Chem 1988;263:14152–14159. [PubMed: 2844759]

Weissert R, Wallstrom E, Storch MK, Stefferl A, Lorentzen J, Lassmann H, Linington C, Olsson T. MHC haplotype-dependent regulation of MOG-induced EAE in rats. J. Clin. Invest 1998;102:1265–1273. [PubMed: 9739061]

Wekerle H, Kojima K, Lannes-Vieira J, Lassmann H, Linington C. Animal models. Ann. Neurol 1994;36:S47–S53. [PubMed: 7517126]

White SR, Bowker RM. Retrograde transport of horseradish peroxidase is specifically impaired in bulbospinal serotonin axons during experimental allergic encephalomyelitis. J. Neuroimmunol 1988;18:75–86. [PubMed: 2450107]

Zhu B, Luo L, Moore GR, Paty DW, Cynader MS. Dendritic and synaptic pathology in experimental autoimmune encephalomyelitis. Am. J. Pathol 2003;162:1639–1650. [PubMed: 12707048]

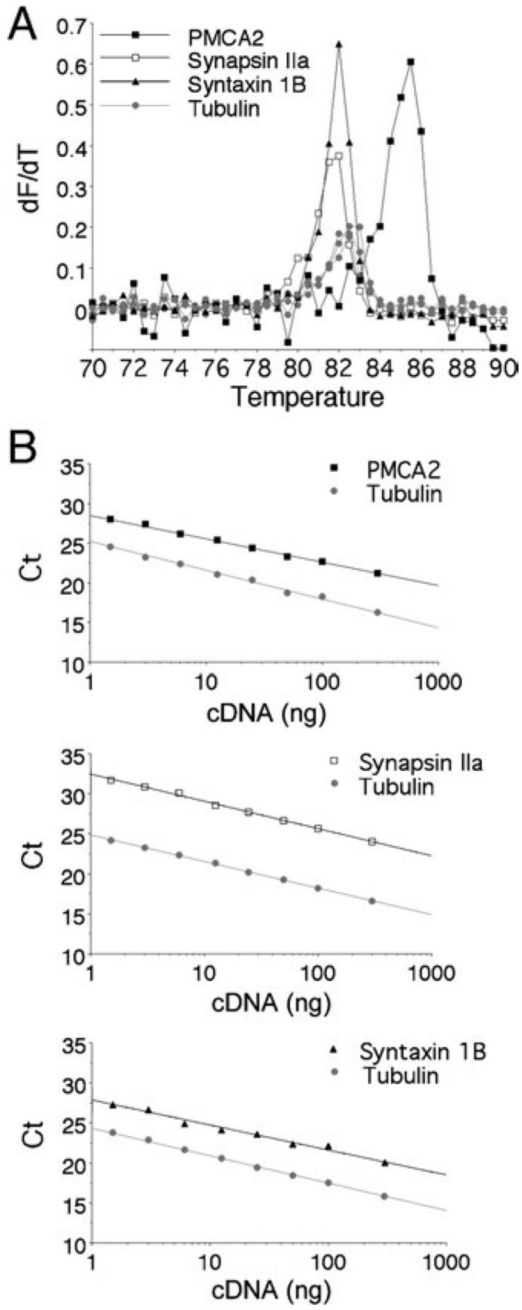

Fig. 1.

Assessment of real-time quantitative multiplex PCR using LUX fluorogenic primers. Complementary DNA template synthesized from spinal cord mRNA was analysed for target (PMCA2; synapsin IIa or syntaxin 1B) transcript levels using FAM-labelled specific primers and simultaneously for α-tubulin transcript level using a JOE-labelled primer. (A) Representative melting curves [temperature vs. fluorescence (d*F*/d*T*)]. The uniqueness of the amplicon synthesized after PCR using the FAM-labelled target primers and the JOE-labelled alpha-tubulin primer were assessed by melting analysis. Ramping of the temperature to 90 °C produced a single unique DNA dissociation curve at 82–85 °C for each fluorescence channel. (B) Real-time PCR standard curves. Wells containing serial dilutions of total cDNA template (300–1.5 ng) were assayed to generate a standard curve for target and alpha-tubulin transcripts.

The Ct for each dilution is determined and expressed as a function of total cDNA loaded. The standard curves demonstrate a wide dynamic range that was linear over at least two orders of magnitude. The linear regression correlation coefficient for each curve is > 0.98, and the slope (indicating efficiency) approximates 3.1 for PMCA2, 3.4 for synapsin IIa, 3.2 for syntaxin 1B and 3.3–3.4 for α-tubulin. As the slopes for target and α-tubulin transcripts were similar (difference < 0.4), transcript relative levels in experimental samples were further calculated from the respective Ct values for target gene and α-tubulin using the 2-ΔΔCt method.

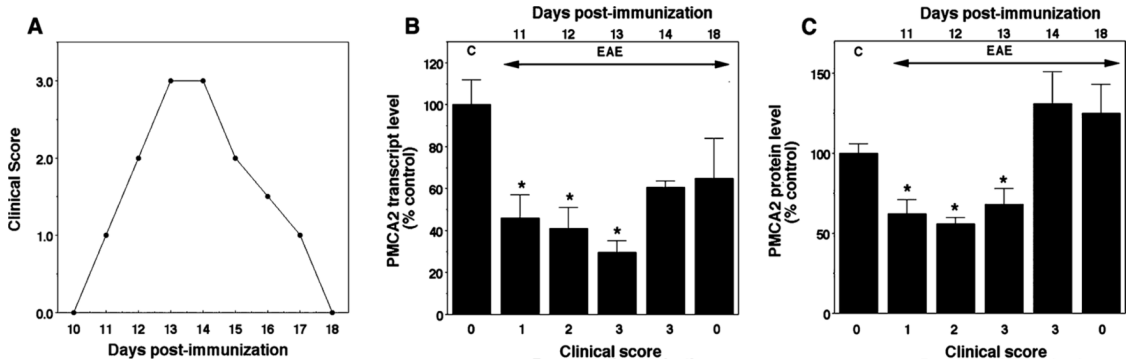

Fig. 2.

Expression of PMCA2 mRNA and protein levels in the lumbar spinal cord during the course of acute EAE in the Lewis rat. (A) Clinical course of the disease. Score 0, no symptoms; 1, flaccid tail; 2, paralysis of one hindlimb; 3, paralysis of both hindlimbs. (B) PMCA2 transcript levels assessed by real-time PCR. C stands for control, animals immunized only with adjuvant. (C) PMCA2 protein levels assessed by western blot analysis. *$P < 0.05$, compared with control.

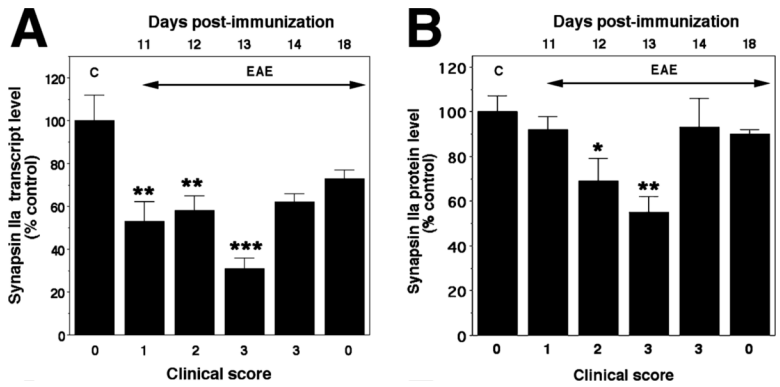

Fig. 3.

Expression of synapsin IIa mRNA and protein levels in the lumbar spinal cord during the course of acute EAE in the Lewis rat. (A) Synapsin IIa transcript levels assessed by real-time PCR. C stands for control, animals immunized only with adjuvant. (B) Synapsin IIa protein levels assessed by western blot analysis. ***$P < 0.001$; **$P < 0.01$; *$P < 0.05$, compared with control.

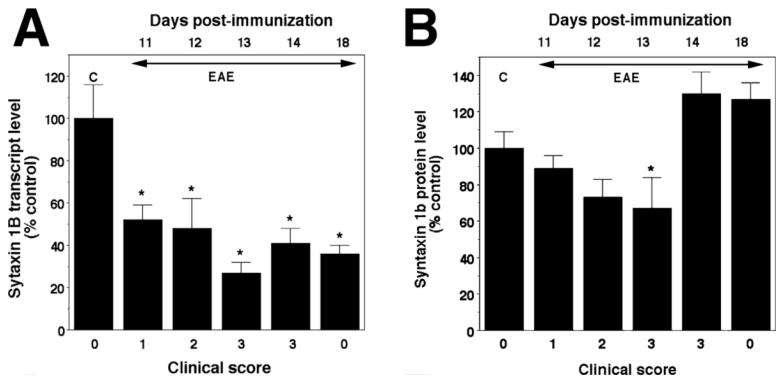

Fig. 4.

Expression of syntaxin 1B mRNA and protein levels in the lumbar spinal cord during the course of acute EAE in the Lewis rat. (A) Syntaxin 1B transcript levels assessed by real-time PCR. C stands for control, animals immunized only with adjuvant. (B) Syntaxin 1B protein levels assessed by western blot analysis. Significantly different from control $*P < 0.05$.

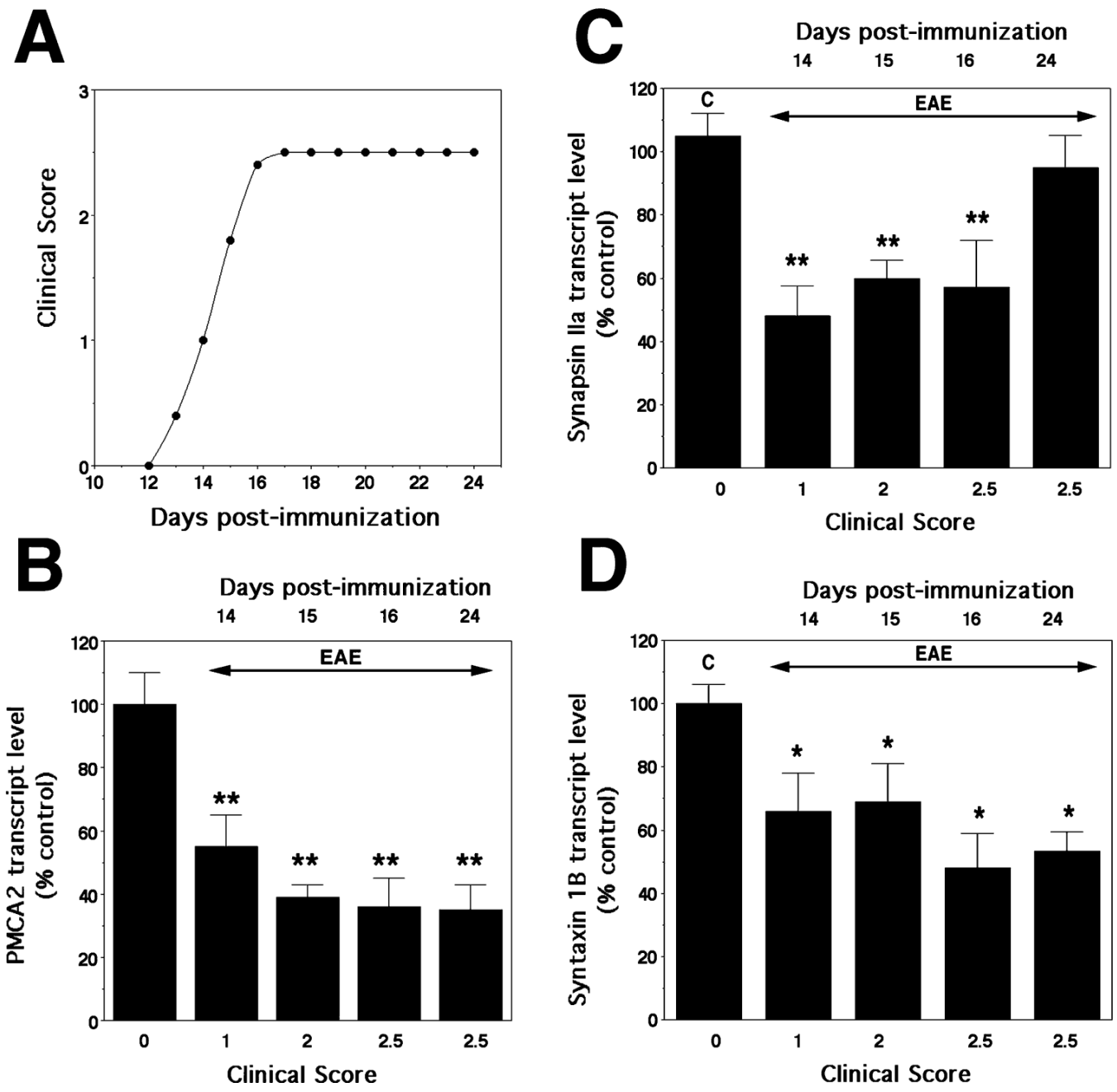

Fig. 5.

Expression of PMCA2, synapsin IIa and syntaxin 1B mRNA in the lumbar spinal cord of C57Bl/6 mice during the course of MOG-induced EAE. (A) Clinical course of the disease. Score 0, no symptoms; 1, flaccid tail; 2, one hindlimb paralysis; 3, paralysis of both hindlimbs. (B) PMCA2 transcript levels assessed by real-time PCR. C stands for control, animals immunized only with adjuvant. (C) Synapsin IIa transcript levels assessed by real-time PCR. (D) Syntaxin 1B transcript levels assessed by real-time PCR. $^{**}P < 0.01$; $^{*}P < 0.05$, compared with control. Note that PMCA2, synapsin IIa and Syntaxin 1B transcript levels are significantly reduced at onset of symptoms, similar to that observed in acute EAE in the rat.

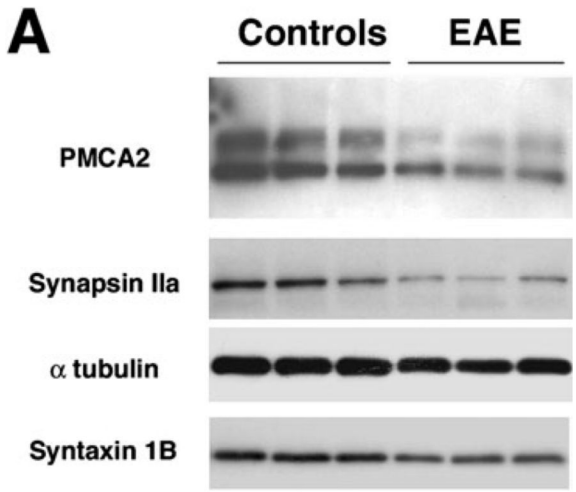

B

	Control	EAE
PMCA2	100 ± 8	40 ± 19 **
Synapsin IIa	100 ± 8	60 ± 17 *
Syntaxin 1B	100 ± 4	89 ± 3

Fig. 6.

Immunoblot analysis of PMCA2, synapsin IIa, syntaxin 1B protein levels in the lumbar spinal cord of control and EAE (day 24 PI) C57Bl/6 mice. (A) Representative western blot. Protein obtained from the lumbar spinal cord of each individual mouse was loaded on separate lanes. Two major bands for PMCA2 (between 130 kDa and 145 kDa), a 78-kDa band for synapsin IIa and a 35 kDa band for syntaxin 1B are vizualized in accordance with the expected size of these proteins. The PMCA2 bands correspond to PMCA2 splice isoforms (Stauffer *et al*., 1993) and to different degree of oxidation of PMCA2 obtained in Tris-Gly gels (A. Nicot & S. Elkabes, unpublished observations). α-tubulin (50 kDa) was used as an internal control. The experiment was performed twice and yielded similar results. (B) Relative PMCA2, synapsin IIa and syntaxin 1B levels in the lumbar spinal cord of controls and EAE (clinical score 3, day 24 PI) C57B/6 mice assessed by western blot analysis. The results are expressed as percentage of control and represent mean ± SEM ($n = 4$) after normalization to α-tubulin. $^{**}P < 0.01$, $^{*}P < 0.05$, compared with control.

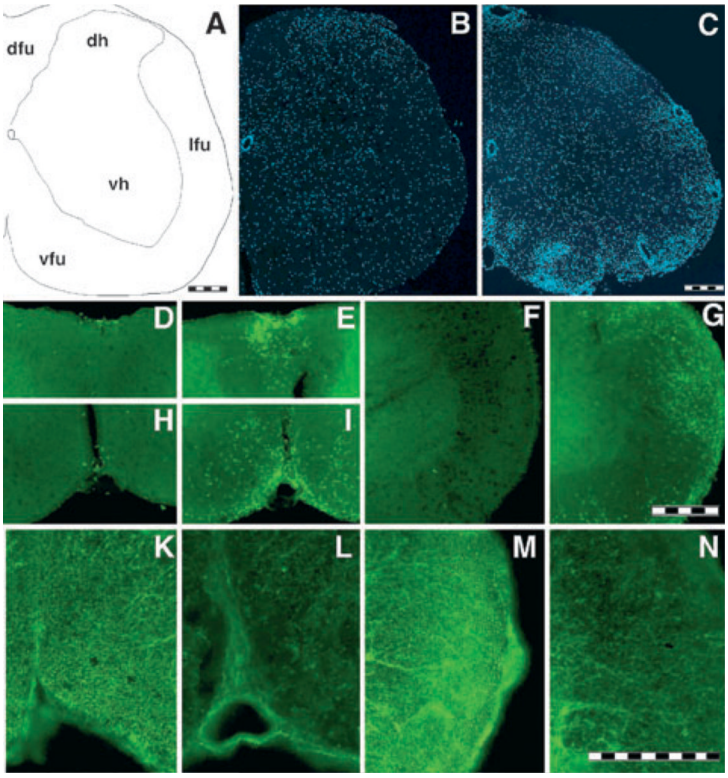

Fig. 7.

Correlation between inflammatory cell infiltration and reduction in PMCA2 immunoreactivity in MOG-induced EAE in C57Bl/6 mice. (A) Schematic drawing of a hemisection indicating the different regions of the spinal cord. dfu, dorsal funiculus; dh, dorsal horn of the grey matter; lfu, lateral funiculus; vfu, ventral funiculus; vh, ventral horn of the grey matter. (B and C) DAPI staining showed increased cell density in the white matter of the EAE mouse (C; 24 day PI, clinical core 3) as compared to complete Freund's adjuvant/PBS-injected control (B). (D–G) CD4 immunostaining showing lymphocyte infiltration in EAE mouse (E, G and I) and controls (D, F and H). The regions shown are dorsal funiculus (D and E), lateral funiculus (F and G) and ventral funiculus (H and I). (K–N) PMCA2 immunostaining showing decreased labelling in axon bundles of the ventral funiculus (L) or lateral funiclus (N) as compared to control mice (K and M, respectively). Lumbar spinal cord coronal sections (40-μm thick) were used. Scale bars, 200 μm (A–C, D–I, K–N).

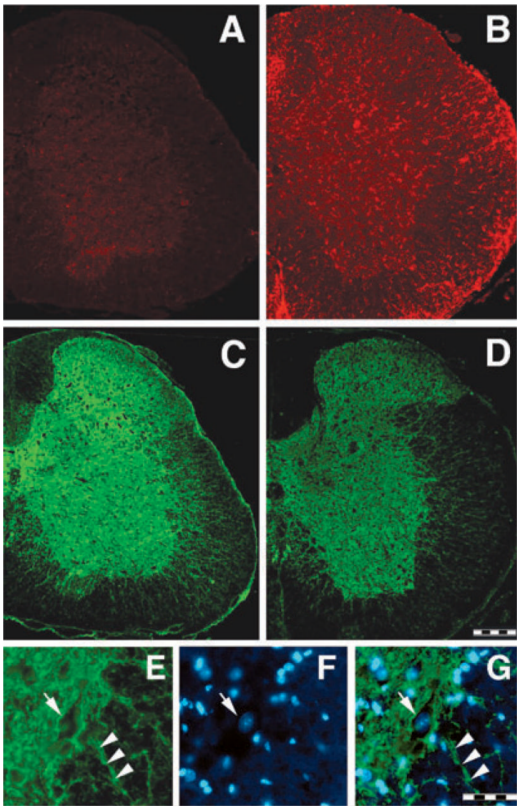

Fig. 8.

Mac-1 (A and B) and PMCA2 (C, D and E) immunostaining in lumbar spinal cord coronal sections in controls (A, C and E) and EAE (B and D) mice. Expression of Mac-1, a marker of microglia/macrophages, is increased throughout the whole lumbar spinal cord in EAE animals (day 24 PI) while the intensity of PMCA2 labelling is reduced. PMCA2 immunostaining is mainly localized to grey matter, with some labelled processes penetrating the ventral and lateral funiculi. (E–G) High magnification picture of PMCA2 (E), DAPI staining (F) and merged stainings (G) at the grey matter/white matter interface showing PMCA2 immunostaining on neuronal membrane (E, G, arrow) and some processes penetrating the white matter (E, G, arrowhead). Arrow in F indicates a typical neuronal nucleus stained with DAPI. Scale bar, 200 μm (A–D); 50 μm (E–G).

Table 1

Relative levels of PMCA1, 3 and 4 mRNA in lumbar spinal cord of controls and EAE (day 13 PI, peak of disease) Lewis rats assessed by RT-PCR

	mRNA, as percentage of control	
	Controls	**EAE**
PMCA1	100 ± 7	110 ± 11
PMCA3	101 ± 2	110 ± 20
PMCA4	100 ± 11	97 ± 10

The results are expressed as percentage of control (mean ± SEM, $n = 3$) after normalization to α-tubulin, a housekeeping gene whose expression is not modified during EAE.